Int. J. Electrochem. Sci., 17 **(2022)** Article Number: 220221, doi: 10.20964/2022.02.21

International Journal of
ELECTROCHEMICAL
SCIENCE
www.electrochemsci.org

Preparation of Mn_3O_4 Nanoparticles via Precipitation in Presence of CTAB Molecules and Its Application as Anode Material for Lithium Ion Batteries

*Lin-Hui Wang[1, #], Long-Long Ren[2, #], Yu-Feng Qin[1, *], Jun Chen[1], Hong-Ye Chen[1], Kai Wang[3], Heng-Jun Liu[4], Zhe Huang[5], and Qiang Li[4, *]*

[1] College of Information Science and Engineering, Shandong Agricultural University, Taian, Shandong, 271018 P. R. China.
[2] College of Mechanical and Electronic Engineering, Shandong Agricultural University, Taian, Shandong, 271018 P. R. China.
[3] College of Electrical Engineering, Qingdao University, Qingdao 266071, P. R. China.
[4] College of Physics, University-Industry Joint Center for Ocean Observation and Broadband Communication, Qingdao University, Qingdao 266071, P. R. China.
[5] Wuhan Maritime Communication Research Institute, Wuhan, Hubei, 430205 P. R. China.
[#]Co-first authors:
Lin-Hui Wang and Long-Long Ren contributed equally to this work.
[*]E-mail: qinyufeng@sdau.edu.cn, liqiang@qdu.edu.cn

Received: 8 October 2021 / *Accepted:* 30 November 2021 / *Published:* 5 January 2022

The Mn_3O_4 nanomaterials were widely investigated due to their potential application as anodes for lithium-ion batteries. Uniform Mn_3O_4 nanoparticles with a suitable diameter of 40 nm were designed and prepared by the water bath method to solve the low conductivity and the pulverization during cycling. The Mn_3O_4 nanoparticles electrodes exhibited an initial discharge capacity of 1288 mAh/g with an initial coulombic efficiency of 65% at 100 mA/g. At 200 mA/g, the reversible capacity increased to 1345 mAh/g after 190 cycles. The specific capacity increased to 547 mAh/g and 691 mAh/g when back to 200 mA/g and 100 mA/g, indicating the exceptional rate capability. The outstanding electrochemical performance of the Mn_3O_4 nanoparticles results from the suitable size of the nanoparticles and the increased conductivity during cycles. The Mn_3O_4 nanoparticles prepared with the water bath method have the potential application as anodes for lithium-ion batteries.

Keywords: Mn_3O_4 nanoparticles, Suitable size, Anodes, Lithium-ion batteries, Increased reversible capacity, Water bath.

1. INTRODUCTION

More and more electric devices, such as mobile phones, tablet computers, electric vehicles, have come into public life and improved the quality of life[1-9]. The energy source of most electric devices

is rechargeable lithium-ion batteries (LIBs) due to their lack of memory effect, environment friendliness, and high energy density[10-19]. Rechargeable LIBs can be used as energy storage devices for solar energy and wind energy, which can reduce the consumption of fossil energy[20-22]. However, the traditional commercial graphite anodes can't meet the further demands of hybrid electric vehicles for their relatively low theoretical capacity[23, 24]. Transition metal oxides have exhibited potential application as anodes for LIBs due to their abundant reserves and high theoretical capacities (500-1000mAh/g)[25-27]. Especially, Mn_3O_4 has attracted much more attention on account of low discharge potential, much lower cost than cobalt and nickel, and high theoretical capacity (937 mAh/g)[28-31]. Nevertheless, to achieve practical application in the future, the intrinsic disadvantages of volume expansion and low electric conductivity(10^{-7}-10^{-8} S/cm) during the cycling process must be dealt with[30, 31]. One general solution is to add carbon-based materials or other conductive species into Mn_3O_4 composite to establish the conductive network of charges and the accommodation buffer of volume variation[32-35]. Ji reported that Mn_3O_4/Graphite powder composite, which was synthesized by an electrochemical method, exhibited a high reversible capacity of 1007.4 mAh/g[32]. Zhao prepared nanorod Mn_3O_4 doped with graphene nanosheets, which showed a high capacity (1155.2 mAh/g) and cycling stability than bare nanorod Mn_3O_4[33]. Shaijumon prepared Mn_3O_4/graphene nanocomposites with nano-octahedron structure, exhibiting a high reversible capacity of 474 mAh/g[34]. Liu prepared a series of Ce-doped Mn_3O_4, which exhibited a high capacity of 754.2 mAh/g after 100 cycles and a good rate capability[35]. Another effective approach is to design and prepare different nanostructures and morphologies to shorten the diffusion length of lithium ions and charges into the active materials[36-39]. Abruna proposed a simple precipitation method to prepare sponge-like nanosized Mn_3O_4, which showed a high reversible capacity of 800 mAh/g[36]. Du reported that order-aligned Mn_3O_4 with a suitable thickness exhibited a high capacity of 637 mAh/g and good cycling stability due to the unique nanostructures[37]. Yang prepared Mn_3O_4 products with different morphologies by tuning the scan rates of the one-step electrochemical method. The spherical like Mn_3O_4 exhibited the best electrochemical results with a reversible capacity of 780 mAh/g[38]. Akhtar prepared porous coral reef-like Mn_3O_4 by a facile hydrothermal procedure, which exhibited a remarkable capacity of 805.2 mAh/g due to the unique structure[39]. Even though most researches focused on the doping of carbon-based materials into Mn_3O_4 composites, the relative good electrochemical results were also obtained by the designing of nanostructures and morphologies. Therefore, it is necessary to explore a facile method to synthesis pure Mn_3O_4 nanomaterials with suitable size and better electrochemical performance.

In this work, uniform Mn_3O_4 nanoparticles with an average size of 40 nm were designed and prepared by the water bath method. Due to the suitable size and the novel preparing method, the Mn_3O_4 nanoparticles electrodes exhibited outstanding electrochemical performance. The high initial discharge capacity of 1288 mAh/g with an initial coulombic efficiency of 65% was obtained at 100 mA/g. The coulombic efficiency sharply increased to 92% and maintained above 95% after the second cycle. At 200 mA/g, the reversible capacity increased from the 50^{th} cycle to the 190^{th} cycle, up to 1345 mAh/g. The specific capacity was 314 mAh/g at 800 mA/g and increased to 691 mAh/g when back to 100 mA/g. The outstanding electrochemical performance of the Mn_3O_4 nanoparticles could result from the suitable size and the increased conductivity during cycles. The Mn_3O_4 nanoparticles with suitable size prepared by the water bath method could be used as anodes for LIBs.

2. EXPERIMENTAL SECTION

2.1 Materials and Methods

The process diagram of preparing Mn_3O_4 nanoparticles is shown in Figure 1. 2 mmol $Mn(CH_3COO)_2{\cdot}4H_2O$ was dissolved in the uniform mixed solution of pure water (21 mL) and dimethylformamide (DMF, 49 mL) by magnetic stirring for 30 seconds and ultrasonic stirring for 2 minutes alternating for several times. 8 mmol hexadecyl trimethyl ammonium bromide (CTAB) was added and followed by another 30 minutes of ultrasonic stirring, and then 10 mmol NaOH was added consequently. The above solution was put into a 60°C water bath and magnetically stirred for 10 minutes to finish the chemical reaction. When naturally cooled to room temperature, the solution was centrifuged with ethanol and pure water, in turn, many times. The obtained precipitates were vacuum dried for 12 h at 60℃, and eventually, the Mn_3O_4 nanoparticles were obtained.

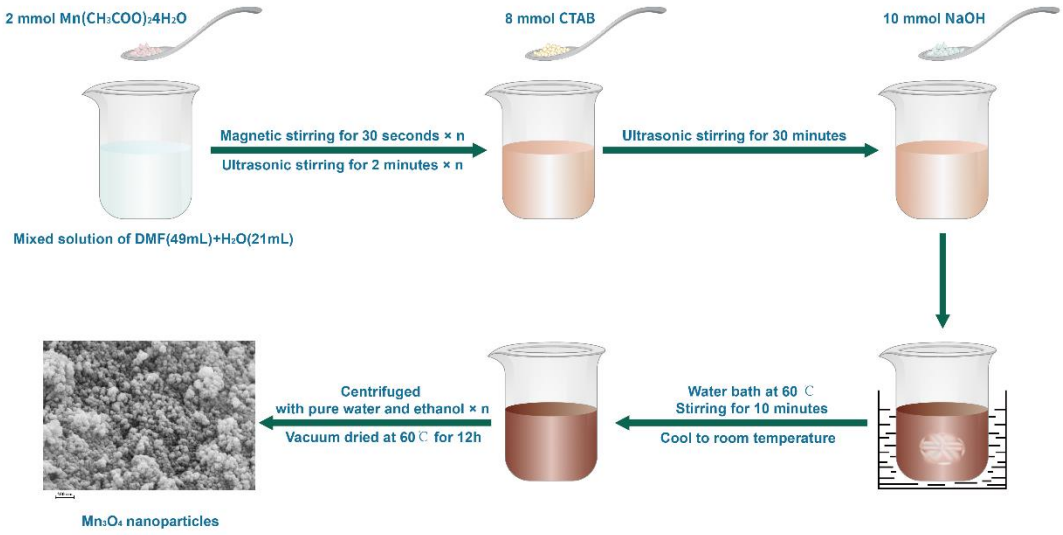

Figure 1. The process diagram of preparing Mn_3O_4 nanoparticles.

2.2 Structure and morphology

The structure was characterized by X-ray diffraction (XRD, Smart Lab, Rigku Japan) in the range of 10° to 70°using a Cu Kα radiation. The morphology was further identified by a scanning electron microscope (SEM, GeminiSEM300, Zeiss, Germany).

2.3 Electrochemical performance characterization

The anode materials were mixed with Mn_3O_4 nanoparticles (70wt%), carbon black (20wt%), and carboxymethyl cellulose (10wt%) aqueous solution. The mixed paste was uniformly coated on a copper collector and vacuum dried at 60℃ overnight. Finally, the coated collector was punched into disks to

assemble the half-cells (CR-2032) as electrodes. The lithium metal disk and the Celgard 2250 film were used as the counter electrode and the diaphragm in the half cells. The electrolyte was 1M LiPF6 dissolved in ethyl carbonate (50v/v%) and dimethyl ethyl carbonate (50v/v%) mixed solution. The electrochemical performance and impedance characteristics were measured by battery measuring systems (Land-ct2001A, China) and electrochemical workstation (CHI660E, China) in the potential range of 0.01 V-3.0 V at room temperature.

3. RESULTS AND DISCUSSION

3.1 Structure and morphology

The XRD patterns of as-prepared precipitates consist with the standard card of PDF No. 24-0734 (Mn_3O_4), as is shown in Figure 2(a). There are no other diffraction peaks observed, which indicates the purity of Mn_3O_4 products. The characteristic peaks located at 18.0°, 29.0°, 32.5°, 36.2°, 38.1°, 44.5°, 50.8°, 58.5°, 60.0°, and 64.7° correspond to (101), (112), (103), (202), (004), (220), (105), (321), (224), and (400) crystal plane of the tetragonal Mn_3O_4 phase respectively, indicating a good crystallinity of Mn_3O_4[27, 29-32]. To further identify the morphology of the Mn_3O_4 products, the SEM image with a scale bar of 200 nm is shown in Figure 2(b). The Mn_3O_4 products are uniform nanoparticles with an average diameter of 40 nm.

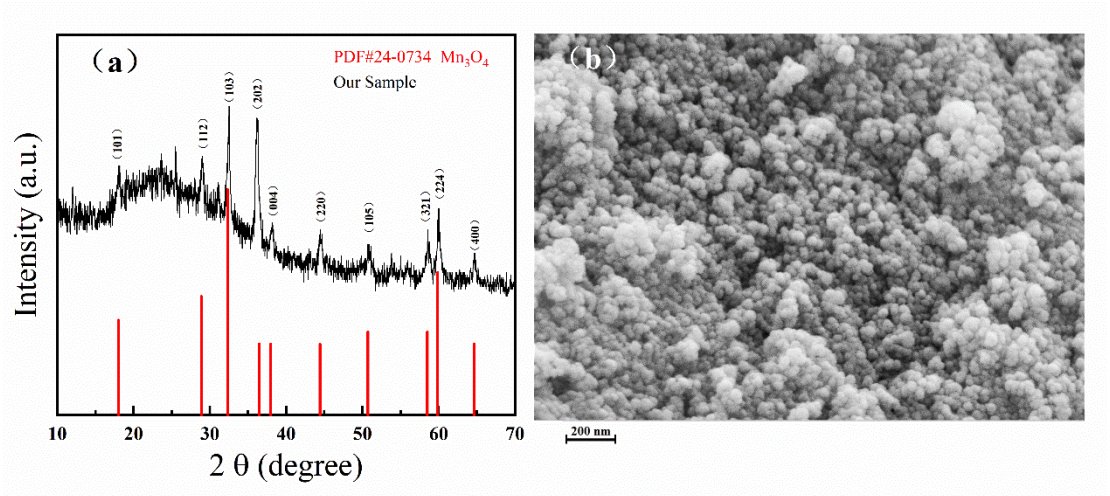

Figure 2. The XRD patterns (a) and the SEM images (b) of Mn_3O_4 nanoparticles.

3.2 Electrochemical Performance

The first five cyclic voltammetry (CV) curves of Mn_3O_4 particles at 0.1 mV/s were shown in Figure 3(a) to clarify the electrochemical reaction mechanism. There is a broad reduction peak at 1.30V accompanied with two minor peaks (only can be seen when partial magnification) at 1.55 and 0.85V in the first cathodic sweep, which corresponds to the formation of solid electrolyte interface (SEI) layer,

the decomposition of electrolyte, and the reduction reaction of Mn_3O_4 to MnO[23, 28, 29, 31, 33]. These broad peaks almost disappear after the first cycle due to the stability of the SEI layer, which is beneficial for the discharge-charge cycling stability[29, 31, 33]. There is also a sharp reduction peak at 0.13 V, which strongly relates to the reductive process of Mn_3O_4 to Mn[23, 27-29]. In the second sweep, the sharp reduction peak splits into two peaks located at 0.38 and 0.27V, corresponding to the details of reduction of Mn_3O_4 to MnO and the further reduction process to Mn[28, 35, 38]. After the third sweep, the main reduction peak of Mn_3O_4 to Mn was determined at 0.37V due to the improved kinetic after litigation and modification of the structure, which indicates the stable reduction reaction process of Mn_3O_4 to Mn in the subsequent cycles[32-34, 38, 39]. While for the anodic sweeps, two broad oxidation peaks located at 1.35 and 2.45V are obvious, which are consistent with the reductions process of Mn to MnO accompanying the decomposition of LiO_2 and the further reaction of MnO to Mn_3O_4[28, 29, 33, 38]. The two oxidation peaks are almost coincident in the five anodic sweeps, which indicates the relatively stable electrochemical reaction and the cycling stability[36-38].

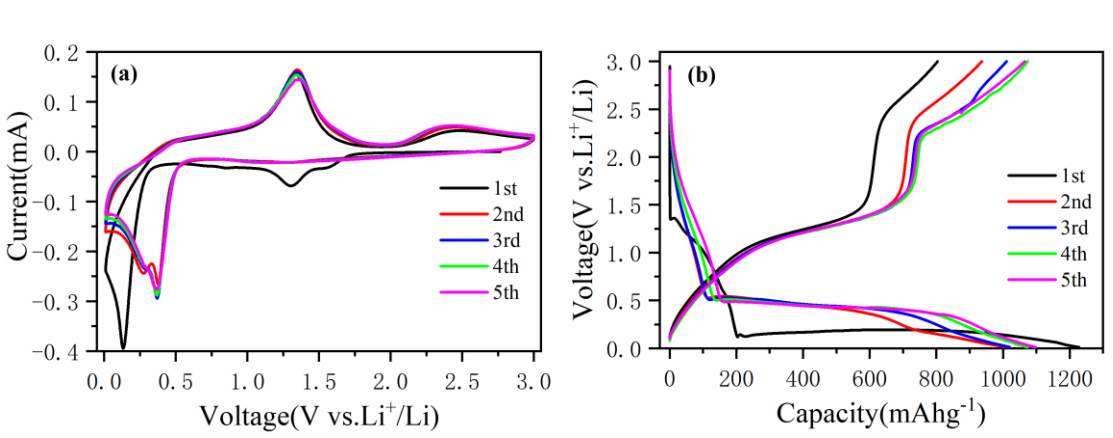

Figure 3. The first five CV curves (a) at 0.05 mV/s and discharge-charge curves (b) at 100 mA/g for Mn_3O_4 nanoparticles.

In order to compare the results of CV curves, the first five charge-discharge curves of Mn_3O_4 nanoparticles at 100 mA/g were measured, as is shown in Figure 3(b). In the first discharge curve, there are two discharge plateaus around 1.36–0.25V and 0.14-0.01V, which consist with the reduction peaks of 1.30 and 0.13V in the initial CV cathodic sweep. In the following discharge process, the plateau increases to 0.52-0.3V, which corresponds to the increase of reduction peak to 0.35V in the cathodic CV sweeps. In the first charge curve, the two charge platforms around 1.00-1.53V and 2.42-3.00V strongly relate to the oxidation peaks of 1.35 and 2.45V in the initial CV anodic sweep. After the second cycle, the shapes of the charge-discharge curve are similar, indicating the same and stable electrochemical reaction process[35-37]. From Figure 3(b), the initial discharge and charge capacities are 1288 and 804 mAh/g with an initial coulombic efficiency of 65%. The loss of the charge capacity could be due to the formation of the SEI layers. The coulombic efficiency increases to 92% in the second cycle and remains above 95% in the following cycles.

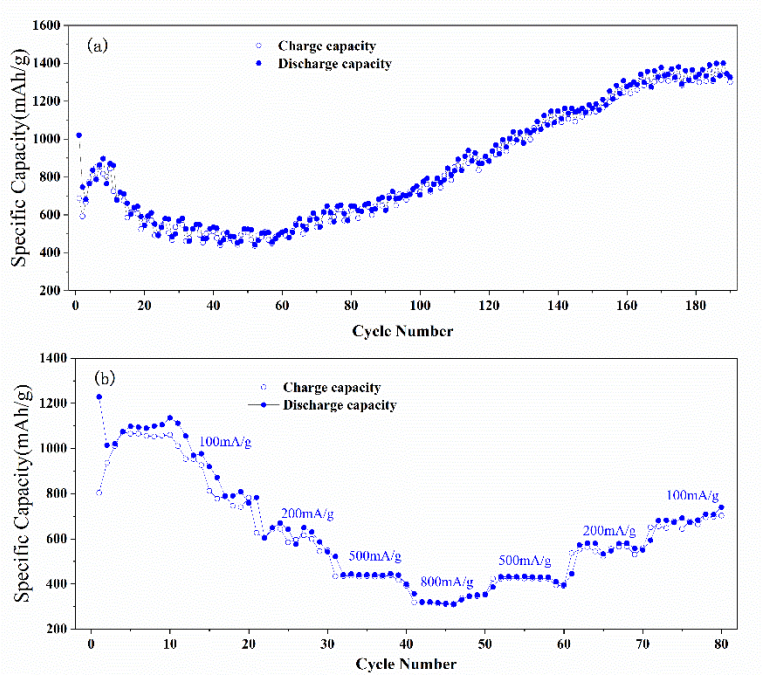

Figure 4. The cycle stability (a) at 200 mA/g and the rate capability (b) for Mn_3O_4 nanoparticles.

The cycle performance at 200mA/g and the rate capability at different current densities of Mn_3O_4 nanoparticles were also measured. According to Figure 4(a), the reversible capacity increases in a few cycles first and decreases from 10^{th} to 50^{th} cycles, and then gradually increases to 200^{th} cycle, which is much common for transition metal oxides anodes[28, 40, 41]. The first increase of capacity could be ascribed to the active process of Mn_3O_4 nanoparticles in the first redox reaction cycles[28, 40], and the subsequent decrease could be due to the evolution of the SEI layers and the insufficient reaction of some active sites[38, 39, 41]. While for the increase during the following cycles, the increase of the active sites and the pseudocapacitive effect should be the reasons, which could result from the polymeric gel-like layer and the structural transformation from crystal to amorphous of Mn_3O_4 nanoparticles during the discharge-charge cycles[11, 28, 39-42]. The comparison of our electrochemical results of Mn_3O_4 nanoparticles electrodes and these of other reported Mn_3O_4 related anodes is listed in Table 1. The reversible capacity of 1345 mAh/g after 190 cycles was obtained, which is higher than the theoretical capacity and better than most reported Mn_3O_4 material electrodes[32-43].

According to Figure 4(b), the specific capacities of Mn_3O_4 nanoparticles are 1135, 642, 441, and 314 mAh/g at 100, 200, 500, and 800 mA/g, and then increase to 434, 547, and 691 mAh/g when back to 500, 200, and 100 mA/g, which indicates the excellent rate capability due to the suitable size of the Mn_3O_4 nanoparticles. The Mn_3O_4 nanoparticles with a suitable diameter of 40 nm (not too large) not only have a relatively high specific surface area that can provide much more active sites but also can shorten the diffusion length of lithium ions and charges, which can increase the reversible capacity and the rate capability[11, 28-30]. Furthermore, the suitable diameter (not too small) of the Mn_3O_4 nanoparticles can avoid the formation of too many SEI layers, which can effectively utilize the electrolyte and restrain the further decrease of the reversible capacity[40-43].

Table 1. The comparison of our electrochemical results of Mn_3O_4 nanoparticles and these of other reported Mn_3O_4 related anodes.

Materials	Initial Discharge Capacity (mAh/g)	Reversible Capacity (mAh/g)	Current Density (mA/g)	References
Mn_3O_4 nanoparticles	1288	1063 (5 cycles)	100	**This work**
	1021	1345 (200 cycles)	200	
Mn_3O_4/ Fe_3O_4	1510	1040 (200 cycles)	300	[23]
Mn_3O_4/CNF	626.8	566.2 (100 cycles)	0.1C	[24]
Mn_3O_4/rGO	1086.5	677 (150 cycles)	0.1C	[27]
Mn_3O_4/C-N	1956	945 (400 cycles)	1000	[28]
Mn_3O_4/NPCS	2163	1629 (100 cycles)	100	[29]
CNF/Mn_3O_4	1690	760(50 cycles)	100	[30]
Mn_3O_4/C	1422.1	913.8(300 cycles)	500	[31]
Mn_3O_4/Ghp	1209	1007.4 (50 cycles)	100	[32]
Mn_3O_4@GNS	1918.7	1155.2(100 cycles)	100	[33]
Mn_3O_4-rGO	1500	474 (200 cycles)	100	[34]
Mn_3O_4-Ce	1237.8	754.2 (100 cycles)	100	[35]
Mn_3O_4	869	800 (40 cycles)	0.25C	[36]
Mn_3O_4	919	637(100 cycles)	10C	[37]
Mn_3O_4	1517	780 (250 cycles)	1000	[38]
PC-Mn_3O_4	695.2	805.2 (100 cycles)	0.1C	[39]
Mn_2O_3@C	1112 (100 mAh/g)	996 (200 cycles)	0.2C	[40]
MnO/Mn_3O_4	1287 (100 mAh/g)	1007 (560 cycles)	3000	[42]
Mn_3O_4@C	974	473 (50 cycles)	40	[43]

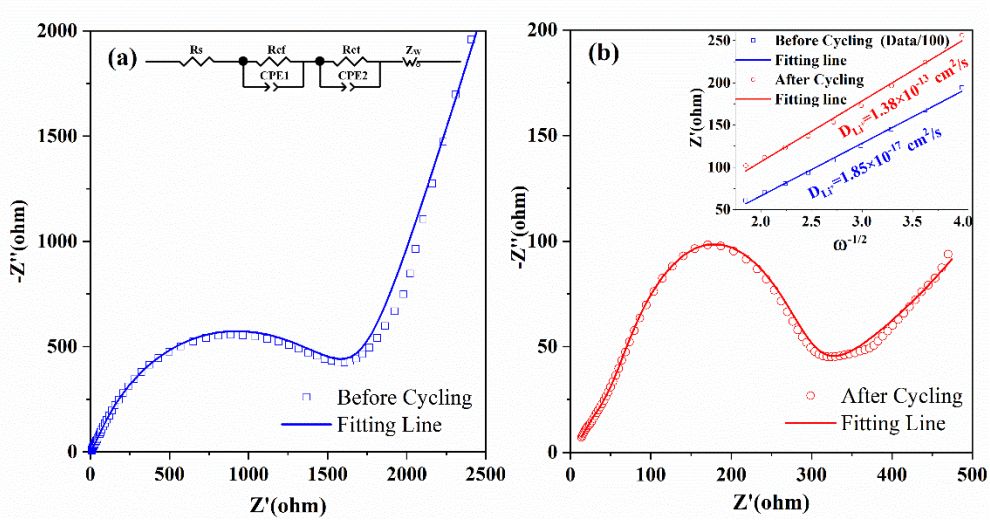

Figure 5. The electrochemical impedance spectroscopy of Mn_3O_4 nanoparticles before (a) and after (b) cycling in the range of 10^{-2} Hz–10^5 Hz.

The electrochemical impedance spectroscopy (EIS) of Mn_3O_4 nanoparticles was measured from 10^{-2} to 10^5 Hz before and after cycling to further verify the reaction kinetics and the enhanced reversible capacity[27-29]. As is shown in Figure 5, both the Nyquist plots (scatters) include two depressed semicircles and a straight line, which can be well fitted by the equivalent circuit (fitting lines) shown in the inset of Figure 5(a). the parameters of R_s, R_{cf}, R_{ct}, and Z_w in the equivalent circuit represent the ohmic

resistance of the electrode and electrolyte, the impedance of the SEI layer, the charge transfer resistance, and the Warburg impedance, respectively[32-34].

$$Z_{real} = R_s + R_{ct} + \sigma\omega^{-1/2} \quad (1)$$

$$D_{Li^+} = \frac{R^2T^2}{2A^2n^4F^4C^2\sigma^2} \quad (2)$$

The Warburg coefficient (σ) can be fitted by Equation (1) according to the EIS data in the low-frequency region, as is shown in the inset of Figure 5(b) with the data of after cycling divided by 100. The Li-ions diffusion coefficient (D_{Li}^+) can be calculated by Equation (2) with the obtained Warburg coefficient σ[11, 27]. The fitted resistance parameters of EIS and the Li-ions diffusion coefficients D_{Li}^+ before and after cycling are presented in Table 2.

Table 2. The fitted resistance parameters of electrochemical impedance spectroscopy and the Li-ions diffusion coefficients before and after cycling.

States	R_s (Ω)	R_{cf} (Ω)	R_{ct} (Ω)	R_{total} (Ω)	D_{Li^+} (cm^2/s)
Before cycling	6.20	11.72	1654	1671.92	1.85×10^{-17}
After cycling	0.75	27.83	200	228.58	1.38×10^{-13}

The R_s, R_{ct}, and R_{total} for Mn_3O_4 nanoparticles are much smaller after cycling, which indicates the increased electric conductivity due to the slight structural transformation and the activation of the materials during the cycling process[44-46]. The relatively low R_s (0.75 Ω), R_{ct} (200 Ω), R_{total} (228.58 Ω) and the high Li-ions diffusion coefficient (1.38×10^{-13} cm^2/s) after cycling indicate the high electrochemical kinetics of the Mn_3O_4 nanoparticles, which are consistent with the outstanding electrochemical performance shown in Figure 4[44-46]. The outstanding electrochemical performance of the Mn_3O_4 nanoparticles could result from the unique structure of the nanoparticle with a suitable diameter of 40 nm and the increased conductivity during discharge-charge cyclesl[40-43].

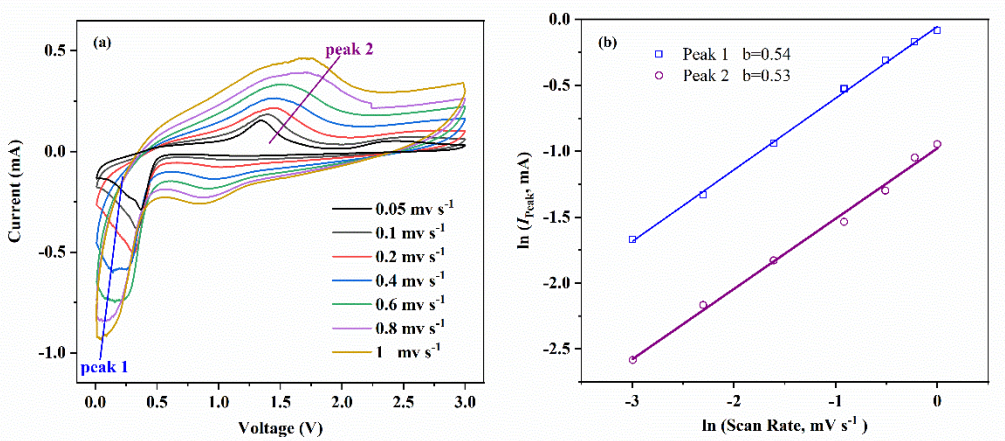

Figure 6. (a) The CV curves of Mn_3O_4 nanoparticles at different scan rates. (b) The values of b according to Equation 4.

As is shown in Figure 6(a), the CV curves of Mn_3O_4 nanoparticles electrodes with increasing scan rates were further measured to identify the lithium-ion storage mechanism. The shapes of the CV curves enlarge with the increase of the scan rates due to different reaction processes[38]. However, the shapes are much similar, and the redox peaks coincide, indicating the outstanding lithium-ion intercalation dynamics and the stability of the electrochemical reaction[38, 42]. The peak current (I_{Peak}) marked by the blue and purple lines can be expressed with scan rates (v) by the equations below.

$$I_{Peak}=a\ v^{b} \quad (3)$$

$$\ln(I_{Peak})= b\ \ln(v) + \ln a \quad (4)$$

Generally, the lithium-ion storage mechanism is contributed by both the diffusion and capacitance-controlled mechanisms with the value of b between 0.5 and 1. When b=0.5, the diffusion-controlled mechanism is dominant, while for b=1, the capacitance-controlled mechanism is the main contribution. According to Figure 6(b), The values of b for the reduction peak and oxidation peak are 0.54 and 0.53, indicating the dominant diffusion-controlled mechanism, which is consistent with the suitable diameter of the nanoparticles and the short diffusion length lithium-ions and the charges.

4. CONCLUSION

The nanostructures and morphologies of the active materials are very important for the electrochemical performance of the electrodes. In this work, the Mn_3O_4 nanoparticles with a suitable diameter of 40nm were designed and prepared by the water bath method. The conductivity of the electrodes was increased largely after cycling due to the suitable size of Mn_3O_4 nanoparticles, which could improve the lithiation and delithiation process. The Mn_3O_4 nanoparticle electrodes exhibited high initial discharge and charge capacities of 1288 and 804 mAh/g at 200 mA/g, respectively. After 190 cycles, the reversible capacity increased to 1345 mAh/g. The specific capacities changed with the current densities and increased to 547 and 691mAh/g when the current densities went back to 200 and 100 mA/g. The outstanding electrochemical performance of the Mn_3O_4 nanoparticles could result from the suitable size of the nanoparticles and the increased conductivity during cycles. The Mn_3O_4 nanoparticles prepared with the water bath method could be used as anodes for the next generation LIBs.

ACKNOWLEDGMENTS
This work was supported by the National Natural Science Foundation of China No. 22179066 and a Project of Shandong Province Higher Educational Science and Technology Program No. J17KA184.

References

1. Q. Li, H. Li, Q. Xia, Z. Hu, Y. Zhu, S. Yan, C. Ge, Q. Zhang, X. Wang, X. Shang, S. Fan, Y. Long, L. Gu, G.-X. Miao, G. Yu, J. S. Moodera, *Nat. Mater.,* 20 (2021) 76-83.
2. H. Li, Z. Hu, Q. Xia, H. Zhang, Z. Li, H. Wang, X. Li, F. Zuo, F. Zhang, X. Wang, W. Ye, Q. Li, Y. Long, Q. Li, S. Yan, X. Liu, X. Zhang, G. Yu, G. X. Miao, *Adv. Mater.,* 33 (2021) 2006629.
3. X. Luo, F. Zhang, Q. Li, Q. Xia, Z. Li, X. Li, W. Ye, S. Li, C. Ge, *J. Phys.: Condens. Matter,* 32

(2020) 334001.
4. F. Zhang, X. Teng, W. Shi, Y. Song, J. Zhang, X. Wang, H. Li, Q. Li, S. Li, H. Hu, *Appl. Surf. Sci.*, 527 (2020) 146910-146920.
5. Y. Zhou, Y. Wang, K. Wang, L. Kang, F. Peng, L. Wang, J. Pang, *Appl. Energy*, 260 (2020) 114169-114184.
6. K. Wang, L. Li, T. Zhang, Z. Liu, *Energy*, 70 (2014) 612-617.
7. W. Kai, F. Xiao, P. Jinbo, R. Jun, D. Chongxiong, L. Liwei, *Int. J. Electrochem. Sci.*, 15 (2020) 9499-9516.
8. C. Liu, Q. Li, K. Wang, *Renewable Sustainable Energy Rev.*, 150 (2021) 111408.
9. Y. Z. Xiao Feng, Le Kang, Licheng Wang, Chongxiong Duan, Kai Yin, Jinbo Pang, Kai Wang, *Front. Chem. Sci. Eng.*, (2020) https://doi.org/10.1007/s11705-11020-11956-11703.
10. L.-H. Wang, X.-L. Teng, Y.-F. Qin, Q. Li, *Ceram. Int.*, 47 (2021) 5739-5746.
11. L.-H. Wang, Y.-K. Dai, Y.-F. Qin, J. Chen, E.-L. Zhou, Q. Li, K. Wang, *Materials*, 13 (2020) 3797.
12. H. Liang, H. Zhang, L. Zhao, Z. Chen, C. Huang, C. Zhang, Z. Liang, Y. Wang, X. Wang, Q. Li, X. Guo, H. Li, *Chem. Eng. J.*, 427 (2022) 131481.
13. Z. Li, Y. Zhang, X. Li, F. Gu, L. Zhang, H. Liu, Q. Xia, Q. Li, W. Ye, C. Ge, H. Li, H. Hu, S. Li, Y.-Z. Long, S. Yan, G.-X. Miao, Q. Li, *J. Am. Chem. Soc.*, 143 (2021) 12800-12808.
14. S.-F. Li, Z.-Y. Gu, J.-Z. Guo, X.-K. Hou, X. Yang, B. Zhao, X.-L. Wu, *J. Mater. Sci. Technol.*, 78 (2021) 176-182.
15. W.-H. Li, H.-J. Liang, X.-K. Hou, Z.-Y. Gu, X.-X. Zhao, J.-Z. Guo, X. Yang, X.-L. Wu, *J. Energy Chem.*, 50 (2020) 416-423.
16. Z.-Y. Gu, J.-Z. Guo, X.-X. Zhao, X.-T. Wang, D. Xie, Z.-H. Sun, C.-D. Zhao, H.-J. Liang, W.-H. Li, X.-L. Wu, *InfoMat*, 3 (2021) 694-704.
17. X. Hou, W. Li, Y. Wang, S. Li, Y. Meng, H. Yu, B. Chen, X. Wu, *Chin. Chem. Lett.*, 31 (2020) 2314-2318.
18. X. Feng, Q. Li, K. Wang, *ACS Appl. Mater. Interfaces*, 13 (2021) 400-410.
19. J. Zhao, F. Li, Z. Wang, P. Dong, G. Xia, K. Wang, *J. Mater. Sci.: Mater. Electron.*, 32 (2021) 14715-14727.
20. Z. Zhao, Z. Hu, Q. Li, H. Li, X. Zhang, Y. Zhuang, F. Wang, G. Yu, *Nano Today*, 32 (2020) 100870.
21. H. Hu, Q. Li, L. Li, X. Teng, Z. Feng, Y. Zhang, M. Wu, J. Qiu, *Matter*, 3 (2020) 95-126.
22. Z. Zhao, Z. Hu, R. Jiao, Z. Tang, P. Dong, Y. Li, S. Li, H. Li, *Energy Storage Mater.*, 22 (2019) 228-234.
23. D. Zhao, Q. Hao, C. Xu, *Electrochim. Acta*, 180 (2015) 493-500.
24. Y. Zhuang, Z. Ma, Y. Deng, X. Song, X. Zuo, X. Xiao, J. Nan, *Electrochim. Acta*, 245 (2017) 448-455.
25. X. Zhou, J. Shi, Y. Liu, Q. Su, J. Zhang, G. Du, *J. Alloys Compd.*, 615 (2014) 390-394.
26. W. Zhang, H. Wang, Y. Zhang, Z. Yang, Q. Wang, J. Xia, X. Yang, *Electrochim. Acta*, 113 (2013) 63-68.
27. S.-C. Weng, S. Brahma, P.-C. Huang, Y.-C. Huang, Y.-H. Lee, C.-C. Chang, J.-L. Huang, *Appl. Surf. Sci.*, 505 (2020) 144629.
28. L. Li, L. Wang, M. Zhang, Q. Huang, L. Chen, F. Wu, *J. Alloys Compd.*, 775 (2019) 51-58.
29. L. Guo, Y. Ding, C. Qin, W. Song, S. Sun, K. Fang, W. Li, J. Du, F. Wang, *J. Alloys Compd.*, 735 (2018) 209-217.
30. S.-H. Park, W.-J. Lee, *J. Power Sources*, 281 (2015) 301-309.
31. P. Chen, G. Zheng, S. Li, Z. Wang, G. Guo, J. Tang, Z. Wen, S. Ji, J. Cui, J. Sun, *Solid State Ionics*, 338 (2019) 121-126.
32. M. Jing, H. Hou, Y. Yang, Y. Zhang, X. Yang, Q. Chen, X. Ji, *Electrochim. Acta*, 155 (2015) 157-163.

33. L.-L. Wu, D.-L. Zhao, X.-W. Cheng, Z.-W. Ding, T. Hu, S. Meng, *J. Alloys Compd.*, 728 (2017) 383-390.
34. S. P. Varghese, B. Babu, R. Prasannachandran, R. Antony, M. M. Shaijumon, *J. Alloys Compd.*, 780 (2019) 588-596.
35. X. Han, Y. Cui, H. Liu, *J. Alloys Compd.*, 814 (2020) 152348.
36. J. Gao, M. A. Lowe, H. D. Abruña, *Chem. Mater.*, 23 (2011) 3223-3227.
37. J. Wang, N. Du, H. Wu, H. Zhang, J. Yu, D. Yang, *J. Power Sources*, 222 (2013) 32-37.
38. Y. Yang, X. Huang, Y. Xiang, S. Chen, L. Guo, S. Leng, W. Shi, *J. Alloys Compd.*, 771 (2019) 335-342.
39. M. S. Akhtar, P. T. M. Bui, Z.-Y. Li, O. B. Yang, B. J. Paul, S. Kim, J. Kim, A. K. Rai, *Solid State Ionics*, 336 (2019) 31-38.
40. S. Li, B. Li, Y. Zhong, Z. Pan, M. Xu, Y. Qiu, Q. Huang, W. Li, *Mater. Chem. Phys.*, 222 (2019) 256-262.
41. J. Ye, D. Zhao, Q. Hao, C. Xu, *Electrochim. Acta*, 222 (2016) 1402-1409.
42. L.-w. Li, L.-p. Wang, M.-y. Zhang, Q.-z. Huang, K.-j. He, F.-x. Wu, *Transactions of Nonferrous Metals Society of China*, 30 (2020) 1904-1915.
43. C. Wang, L. Yin, D. Xiang, Y. Qi, *ACS Appl. Mater. Interfaces*, 4 (2012) 1636-1642.
44. Z. Li, G. Li, W. Xu, M. Zhou, C. Xu, M. Shi, F. Li, L. Chen, B. He, *ChemElectroChem*, 5 (2018) 2774-2780.
45. J. H. Hong, G. D. Park, D. S. Jung, Y. C. Kang, *J. Alloys Compd.*, 827 (2020) 154309.
46. W. Liu, P. Xiang, X. Dong, H. Yin, H. Yu, P. Cheng, S. Zhang, S. Shi, *Composites, Part B*, 216 (2021) 108883.